KAROL SIEGL*

THE FABRIC OF MESOSCOPIC FOLDS OF DIFFERENT STRUCTURAL REGIMES FROM METAMORPHITES OF THE WESTERN PART OF LOW TATRA Mts. (WEST CARPATHIANS)

(Fig. 1—34)

A b s t r a c t: The fabric of two mesoscopic folds of diverse age and structural level has been studied by means of ac-section morphology, time and space relations of crystallization to the deformation of rock forming minerals and of biotite and quartz subfabrics. The differences between fold fabrics are regarded to be the consequence of diversity of the Variscan and Alpine structural regime.

Р е з ю м е: Внутреннее строение двух малых складок различного возраста и структурного этажа изучено посредством морфологии ас сечения, временных и пространственных отношений кристаллизации к деформации породообразующих минералов и частичных внутренних строений биотита и кварца. Разница между внутренним строением складок подтверждается результатами разницы вариского и альпинского структурного режима.

Introduction

The western part of the Low Tatra Mts. is built up by the Ďumbier crystalline complex of the core-mountain type. Paragneisses with amphibolite intercalations and migmatite make up the mantle of granites and granodiorites. The crystalline complex is overlain by an autochthonous Mesozoic envelope and nappes.

Absolute ages (J. K a n t o r 1959, 1961) and structural relations (K. S i e g l 1970) give evidence for the Variscan dynamothermal metamorphism of the crystalline complex. The effects of Alpine retrograde metamorphism in the level of recent denudation are local, closely related to the tectonogenesis. The folding of the crystalline complex took place during four phases — two Variscan and two Alpine phases.

From the causes determinating the diverse character of the folds the structural level is of special importance. Two cm-folds in gneisses were analyzed in order to elucidate their formation as function of structural level and regime (Fig. 1). The fold F1 originated by Alpine deformation of two-mica paragneisses in the upper structural level. The fold F2 generated during Variscan deformation of banded gneisses in a deeper structural level.

The geometrical analysis and state of strain in the folds

Both folds differ by geographical, orientation and position of the fold axis and surface. F1 is a subhorizontal fold with moderately to steeply inclined axial surface. F2 is a moderately plunging recumbent fold. Both are parts of higher order fold structures. Within the outcrop domain they are assymetric and cylindric.

The utilized geometrical classification is based on the description of folded surfaces on the ac-section by means of orthogonal thickness (J. G. R a m s a y 1967). The

* RNDr. K. S i e g l, CSc., Department of Petrography, Faculty of Natural Sciences of the Comenius University, Bratislava, Gottwaldovo nám. 2.

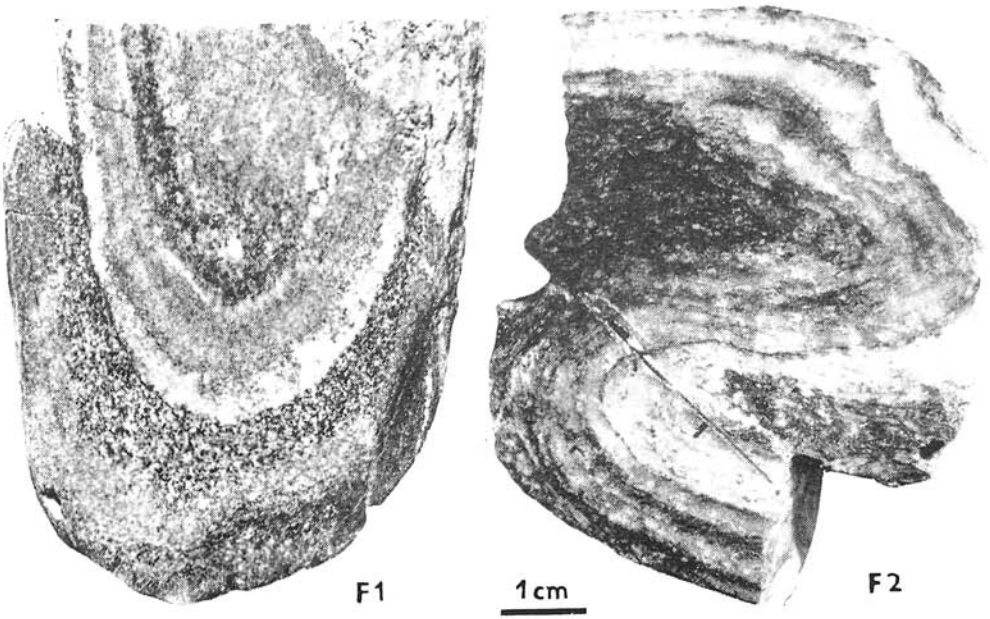

Fig. 1. Folds F1 and F2.

variation in $t' = \frac{t\alpha}{to}$ with the angle α was constructed geometrically for the individual layers of both folds (Fig. 2 and 3).

Fold F1

Two relations are evident from the diagram $t'\alpha$ (Fig. 4): the increase of orthogonal thickness towards the hinge and the different increase in the competent and incompetent layers on behalf of the latter. F1 is a complex fold in which the individual layers were diversely folded. Quartz-plagioclase layers *b*, *bb* belong in Ramsay's classification to the subclass 1C — folds with weakly convergent isogons ($t'\alpha < 1$; $t'\alpha > \cos\alpha$). Biotite layers *c*, *cc* rich in quartz belong partly also to this group. These and the layer *a* are close to the class 2 — folds with parallel isogons ($t'\alpha = \cos\alpha$). To the class 3 — folds with divergent isogons, belongs one part of the biotite layer *aa* near the fold core ($0 < t'\alpha < \cos\alpha$). To this class should belong also the strongly retrograde metamorphosed uncalculated layer of the outer arc.

Assuming the competent layers were buckled into parallel folds and subsequently modified by flattening into similar folds — flattened parallel folds, it is possible to determine from $t'\alpha = (\cos^2\alpha + \frac{\lambda_2}{\lambda_1}\sin^2\alpha)^{1/2}$ the amount of superimposed compressive strain (J. G. Ramsay 1962). The ratio of the principal quadratic extensions λ_1 and λ_2 (parallel and normal to the axial surface), as it has been read from the diagram of $t'\alpha$ values with variations in $\frac{\lambda_2}{\lambda_1}$ in flattened parallel folds

is as follows: for parts close to the hinge of the layer *b*, *bb* $\sqrt{\frac{\lambda_2}{\lambda_1}} = 0{,}9$ up to 0,7, for the layer *c*, *cc* $\sqrt{\frac{\lambda_1}{\lambda_2}} = 0.4$ up to 0.1. The modification of incompetent layers is distinctly stronger. Owing to the tangential longitudinal strain it is impossible to determine the total compressive strain. It is indicated by the low value of t' in the fold limbs and by considerable variations in the particular layers. The general trend of modification of the fold F1 by homogenous strain follows from the subclass 1B towards the class 2.

The incompetent layer of the outer fold arc (uncalculated) has been deformed under formation of shearing cleavage. The curved course of cleavage is due to variation of compress strain in the contact zone of diverse competence layers. Towards the hinge the shear planes are convergent, as it is characteristic for incompetent layers. This part

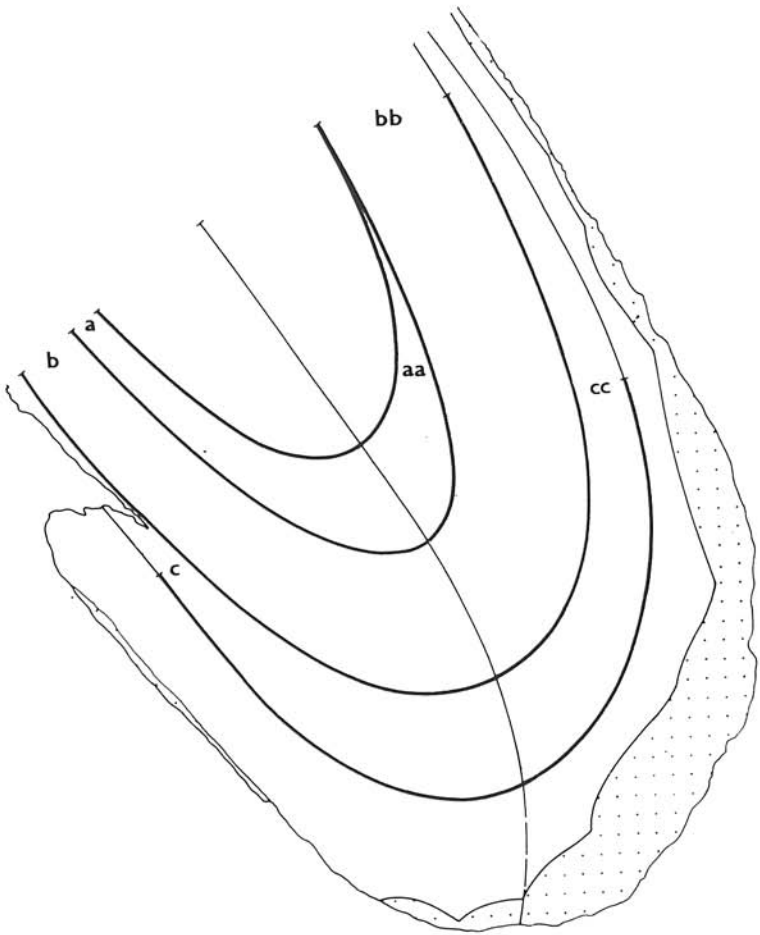

Fig. 2. Shape of ac-section F1. Thick lines mark calculated parts of layers, domain of retrograde metamorphism is dotted.

of the fold suffered by maximal componental movements allied with retrograde recrystallization.

A slip parallel to the boundary as it has been described from plexural slip folds (F. A. Donath 1962), was found between the layers of the outer arc.

Fold F2

In regard to the idealization of biotite-rich layers dispersed by creep in the hinge, the geometrical analysis of this fold is tentative. Only a part of the antiform beside the decollement was calculated.

Plots of $t'\alpha$ (Fig. 5) constructed from the cross section of the antiformal and synformal parts indicate variations of the fold style not only for individual but even in the same layer. So *Sb*, *Sbb* for example has strongly convergent (*Sb* in the subclass 1A).

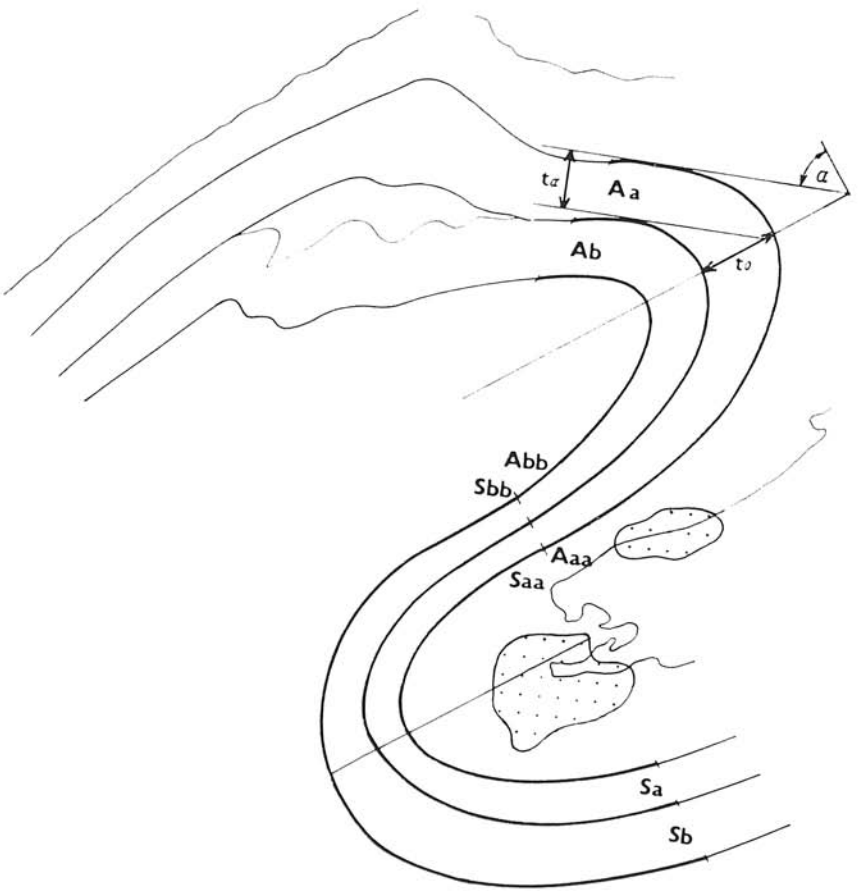

Fig. 3. Shape of ac-section F2 with orthogonal thickness in the hinge (t_o) and in the limb of the antiform (t_2). Thick lines mark calculated parts of layers, domain of retrograde metamorphism is dotted.

but also divergent dip isogons in the synform (*Sbb* in class 3). A considerable part of the cross section shape has weakly convergent dip isogons — subclass 1C. Modification by heterogenous shear parallel to the axial surface is frequent.

In the upper antiform limb and in the synform core structures complicating the fold shape are developed. They generated owing to different rheologic properties of adjacent layers and owing to space reduction in the flexure of the more competent of them. The flexure amplitude in the limb of the antiform decreases towards the core and in the innermost quartz layer three parasitic folds occure. This layer is relatively the most thin and the less competent. Between the layers *Sa* and *Sb* a decollement is originating. The final state of strain in this limb is however similar to that of the whole antiform — dimensional orientation of biotite is identic.

In the synform core deformation effects due tu extreme buckling of the quartz-feldspar layer were also observed. Its material is impressed into the biotite-rich core. The lobate form of the contact is typical for diverse viscosity materials in compression. During the buckling period the quartz-feldspar layer ought to be competent enough to retain creep of the less competent synform core towards the hinge.

The differences in the hinge formation of the antiform and synform of the fold F2 are due to the sequence of the competent layers, their thickness and to the flexure amplitude of the thickest of them.

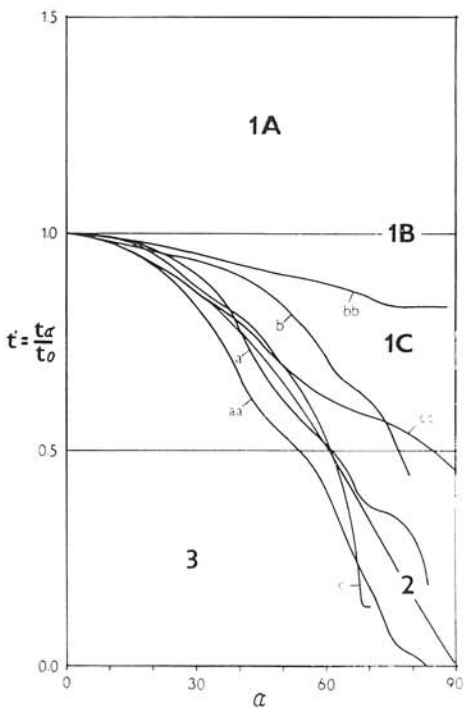

Fig. 4. Plot t_2 of F1.

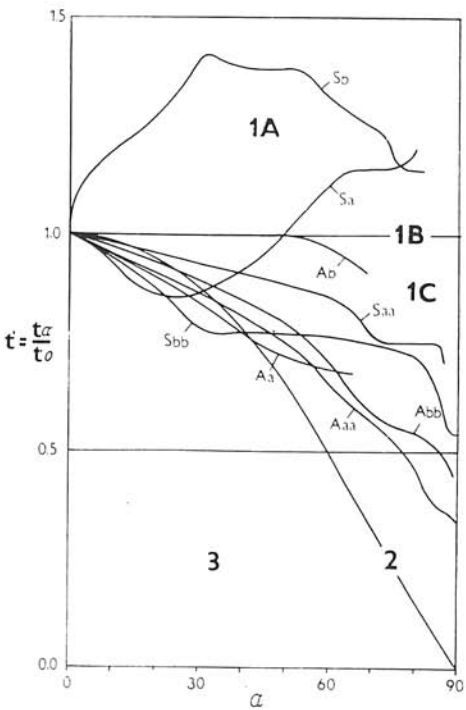

Fig. 5. Plot t_2 of F2.

Mineral composition and its relation to the deformation

The composition of deformed rocks is primary inhomogenous. The state of strain in studied folds is closely related with this feature. Crystallization and recrystallization are controled by the original composition, as well as by the state of strain. In both folds mineral assemblages were found, with different crystallization-deformation relations, belonging to prograde and retrograde metamorphism. In the ideal case the total deformation may be divided into three parts — D_1, D_2, D_3. In both folds only D_1 can be temporarily parallelized. A conspicious discontinuity exists only in F1 between D_1 and D_2.

Fold F1

Within the sample domains of a mineral assemblage with predominating prograde (PMD) and retrograde (RMD) metamorphism can be distinguished. The older assemblage belongs to the garnet amphibolite facies, the younger one to the greenschist facies. RMD are limited to sites of maximal creep, like the incompetent mica-rich layer of the outer arc.

The following minerals were identificated: quartz, biotite, oligoclase, K-feldspar, albite, muscovite, chlorites, garnet, apatite, zircon, zoisite, leucoxene, carbonate. Quartz, muscovite and chlorites are represented by several generations.

Quartz 1 forms xenoblasts (0,1—0,5 mm) aranged in places into glomeroblasts or bands of up to 1,5 mm thickness. The shape of isolated blasts depends on the position and thus also on the posterystalline deformation. In PMD quartz-feldspar layers is lense-shaped, in micaceous layers it is lathy. Undulose extinction is common due to posterystalline deformation D_2.

Quartz 2 appears in PMD in lense-shaped glomeroblasts with straight grain boundaries. Extinction is normal.

Quartz 3 fills up sometimes with carbonates minute fissures. Weak undulose extinction proves for the strain along the fissures.

Biotite is a substantial component of mica-rich layers. Unlike its appearance in quartz-feldspar layers it is bigger (up to 3 mm) with a reddishbrown pleochroism γ. It is often chloritized and sagenitized, in RMD only its relics occur.

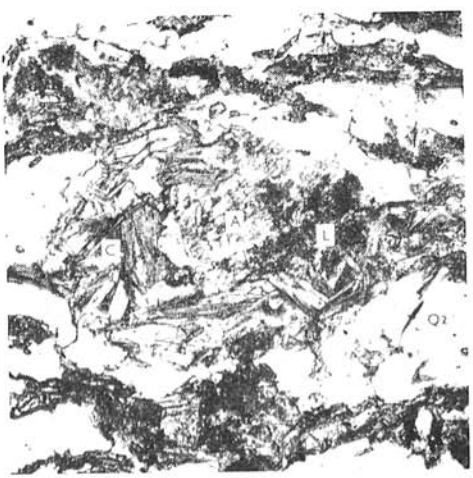

Fig. 6. Retrograde mineral assemblage of F1. Magn. 93 X, N //. Foto L. Osvald. A — albite, C — clinochlor, rhipidolite, L — leucoxene, Q_2 — quartz 2.

Oligoclase An_{20-27} is abundant in quartz-feldspar layers. It encloses micas and quartz 1. It is mostly sericitized and posterystalline deformed.

K-feldspar was found sporadically in PMD, it carries micas and quartz.

Albite together with Mg-chlorites and sericite forms cumuloblasts in RMD. Sporadically synkinematic crystallization with chlorites in *si* is observable, more often it is postkinematic.

Muscovite 1 is more scarce than biotite with which it appears together. One part originated by baueritization.

Muscovite 2 (sericite) is the product of feldspar alteration. By cumulation of minute flakes (less than 0,1 mm) cumuloblasts originate in RMD, filling up the place ofter plagioclase.

Chlorites generated in PMD by biotite and garnet chloritization — pennine, but also by plagioclase and biotite alteration in RMD — clinochlor and rhipidolite. The latter form with sericite, albite and leukoxene characteristic lenseshaped cumuloblasts (Fig. 6).

Garnet was found scarely in the hinge of the layer *a*, *aa*.

The time relations of crystallization of the substantial components to deformation in F1 are represented on the left part of Fig. 7. The maximum of D_1 deformation lies in the range of biotite and muscovite 1 crystallization. The younger deformation D_2 culminated before the main crystalization of muscovite 2, quartz 2, albite and chlorites. During D_1 the parallel fabric of gneiss folded during D_2 generated. Folding was accompanied by direct componental movements and by posterystalline deformation of the components crystallized before D_2. In layers of suitable mineral composition and thus also with maximal action of D_2, a younger crystallization has been induced. The youngest deformation D_3 shows the character of brittle failure.

Fold F2

In the fold sample mineral assemblages and textures of polymetamorphism were found again. Plagioclases are always altered into a fine-grained sericite-chlorite mass, in the core of the synform garnet and younger biotite 2 originated at the same time. The arrangement of garnet accumulations in the strike of the axial surface proves for the alliance of its blastesis with the fold formation.

The following minerals have been identificated: quartz, biotite, muscovite, garnet, chlorites, staurolite, apatite, zircon, carbonates. Quartz and biotite appear in two generations.

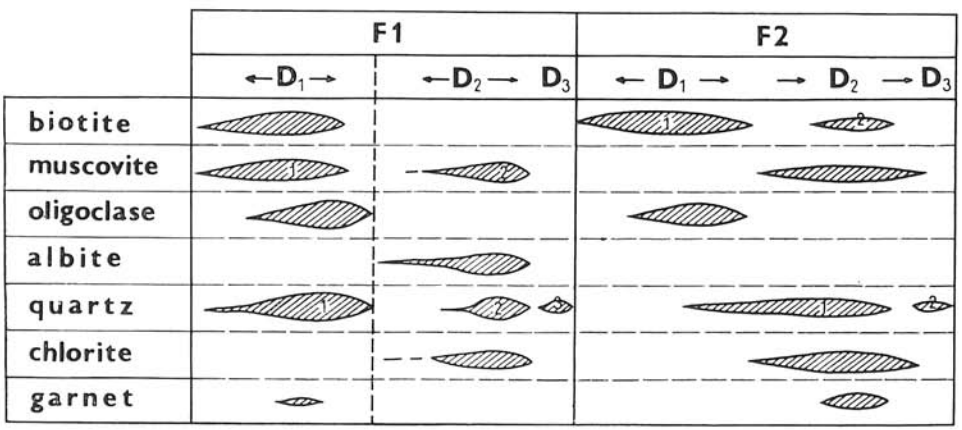

Fig. 7. Sketch of crystallization-deformation relations in F1 and F2.

Quartz 1 forms in quartz-rich layers xenoblasts (less than 7 mm) elongated in the direction of schistosity. Their size decreases towards the hinge. In *si* it contains totally sericitized feldspars, minute idiomorphic biotite flakes and garnet. In biotite-rich layers it is smaller (less than 3 mm), sometimes it makes up lense-shaped glomeroblasts. The grain boundaries in the fold limbs are straight in the flexures sutured.

Quartz 2 originated by recrystallization of quartz 1 in the vicinity of the fissures.

Biotite 1 is in biotite-rich layers on the fold limbs dimensionally oriented in the plane of schistosity. The deviation of smaller flakes from this direction in the hinge domains is in the rule larger owing to direct and indirect componental movements. In the antiform two generations of biotite 1 are distinguishable — a prekinematic and a synkinematic (Fig. 8). In quartz-rich layers biotite is smaller (less than 1 mm), worse oriented and of weaker postcrystalline deformation.

Biotite 2 occurs sporadically in the core of the synform and in the vicinity of the central limb. Poikilitic xenoblasts (more than 0,5 mm) crystallized post kinematically, they carry quartz and sericite. They appear in the rule together with garnet and chlorite and muscovite aggregates in domains of total plagioclase transformation (Fig. 9).

Muscovite originated by plagioclase alteration. It has not been found in the primary form.

Garnet in the mentioned assemblage is not chloritized and postcrystalline deformed unlike the adjacent biotite 1. In times it is atol-like with normal extinction quartz in the centre.

Chlorites are the product of biotite alteration (pennine) and plagioclase transformation (clinochlor).

Calcite fills up fissures in the limb of the antiform (in the maximal stress direction) and synform (in the direction of the convergent cleavage fan).

From the other indentified minerals found in accessory amount staurolite is of close spatial relation to the biotite 2 — garnet assemblage.

The earlier deformation D_1 is homotatactic with schistosity formation in the fold limbs and with a part of buckling. It is tracable by relations to biotite 1 crystallization (Fig. 7). The majority of minerals is to the culmination of D_1 postkinematic, their crystallization was induced by the younger D_2. Final effects of D_2 are observable mainly on one part of quartz 1. During D_2 the folding proceeded, in the hinge zone of the antiform distinct creep traces were found. Fissures filled up with quartz 2 and calcite generated in the state of brittle failure of D_3.

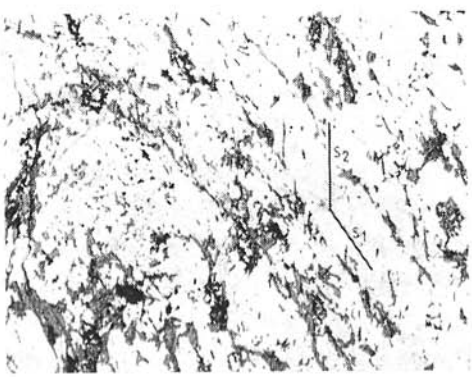

Fig. 8. Fabric of biotite in F2 antiform. Magn. 11 X, N //. Foto L. Osvald.

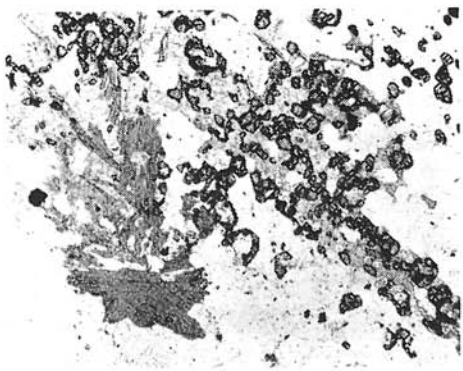

Fig. 9. Garnet and biotite 2 in the retrograde metamorphism domain of F2. Magn. 40 X, N //. Foto L. Osvald.

Subfabrics of biotite

Preferred orientation of biotite has been studied in PMD of both folds by statistical evaluation of normals to {001} cleavage cracks, measured on thin sections from the ac-section (Fig. 10). On F2 both generations of biotite 1 were measured, but not the scarcely appearing biotite 2. The homotaxis of biotite subfabrics with s_1, as well as the grade of their tropic varies in both folds in dependence on the position.

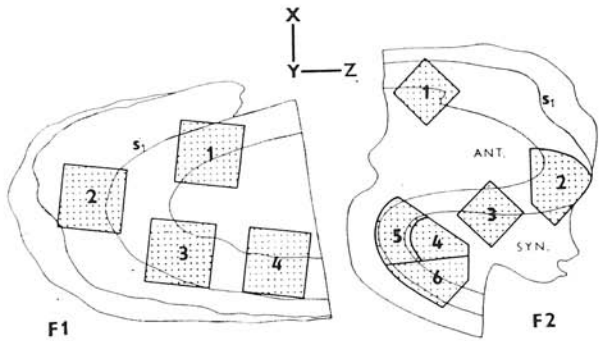

Fig. 10. ac-sections of F1 and F2 with thin section domains of biotite and quartz measurements.

Fold F1

The homotaxis of the biotite subfabric with s_1 decreases proportionally to the incompetence of the sampled layer and to the distance of the hinge. This function is represented by the migration of the maxima on diagrams from the position nearly normal to s_1 to the position when they include a sharp angle ($\sphericalangle M \wedge s_1 = 86°-26°$; Fig. 11 to 14). Biotite in the fold hinge is heterotactic with s_1 — in the direction normal to s_1 the

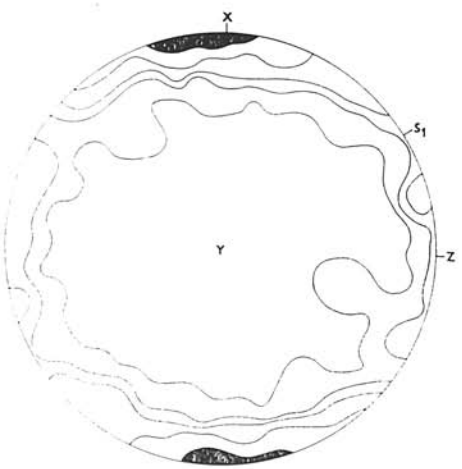

Fig. 11. Biotite, F1-1, 200 poles of {001}, 0—1—2—5—10 < %.

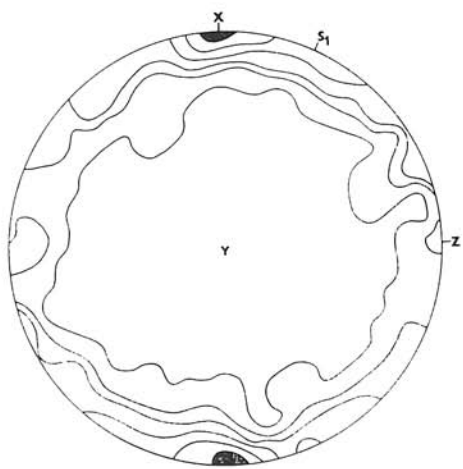

Fig. 12. Biotite, F1—2, 200 poles of {001}, 0—1—2—5—10 < %.

density is less than 1 %. On the thin section from the limb biotite is only weakly posterystalline deformed and reoriented from the position parallel with s_1. It is not strictly parallel with it. the fabric symmetry is only pyramidal rhombic. Biotite reorientation in the hinges of biotitic layers proceed by bending. slippage on {001} and by rotation in the course of direct componental movements during posterystalline deformation D_2.

Comparing the strain orientation in the fold and the diagrams of dimensional orientation of biotite its dependence on the direction of maximal stress is evident. The maximum of the normals to {001} of biotite on the individual thin sections and in the whole

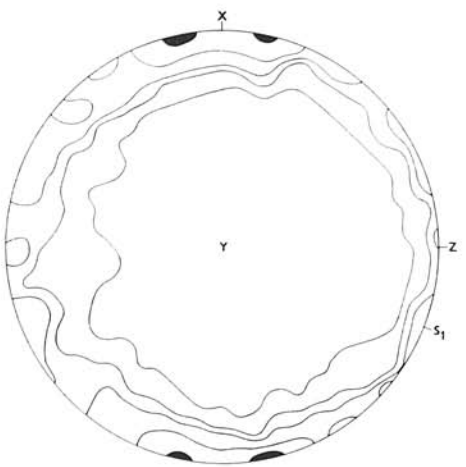

Fig. 13. Biotite, F1—3, 200 poles of {001}, 0—1—2—5—10 < %.

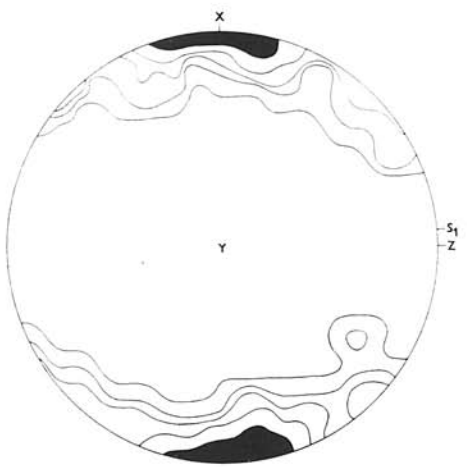

Fig. 14. Biotite, F1—4, 200 poles of {001}, 0—1—2—5—10 < %.

Fig. 15. Biotite, F2—1, 187 poles of {001}, 0—1—2—5—10 < %.

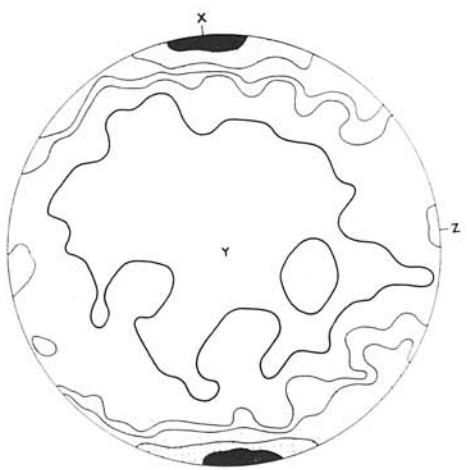

Fig. 16. Biotite, F2—2, 229 poles of {001}, 0—1—2—5—10 < %.

fold (Fig. 20) lies in the direction of the X-axis of the strain elipsoid, i. e. the flakes are reoriented in the hinge into the YZ-plane.

Fold F2

The orientation of biotite on synoptic diagrams of both folds is appearantly similar (Fig. 20 and 21). More detailed revise showed the presence of biotite 1 subfabric homotactic and heterotactic with s_1 in F2. The heterotactic subfabric originated by direct, as well as by undirect componental movements. Heterotactic biotite 1 did either crystallize in the direction of the antiform axial surface, or it was later rotated into it after crystallization. Both cases are conspicuous on the right and left part of Fig. 8. Heterotactic

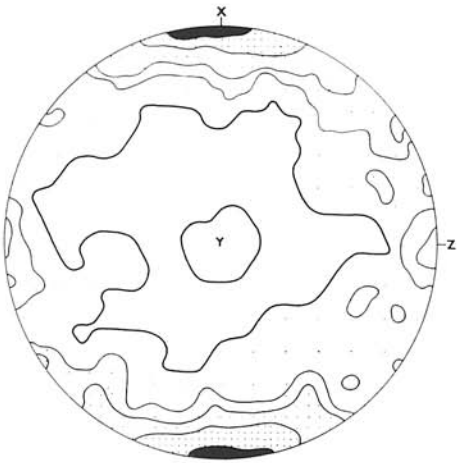

Fig. 17. Biotite, F2—3, 250 poles of {001}, 0—1—2—5—10 < %.

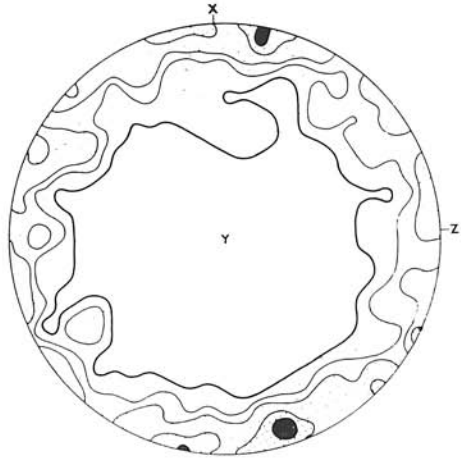

Fig. 18. Biotite, F2—5, 116 poles of {001}, 0—1—2—5—10 < %.

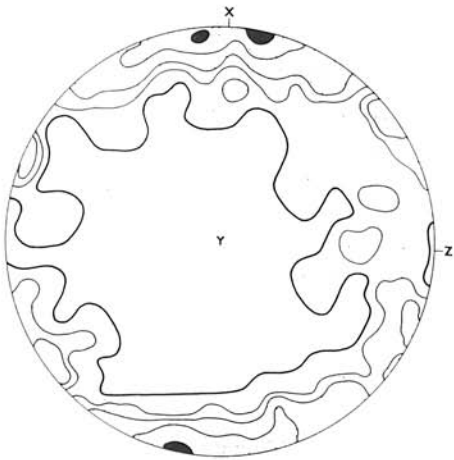

Fig. 19. Biotite, F2—6, 134 poles of {001}, 0—1—2—5—10 < %.

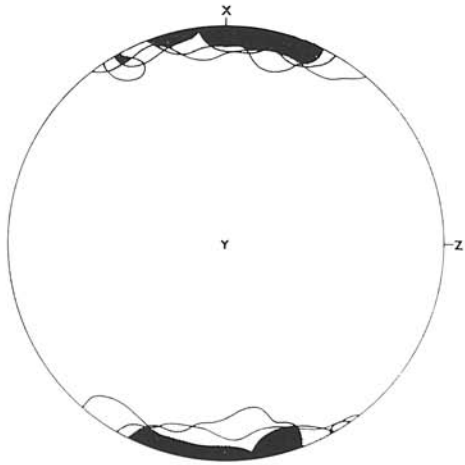

Fig. 20. Biotite, F1—1 to 4, synoptic diagram of 5 % isolines, 800 poles of {001}.

biotite 1 crystallized thus only partly synkinematically with the folding of antiform.

The biotite 1 subfabric in the narrow hinge zone of the antiform was generating similarly as in the F1 — by direct componental movements. In the case of the antiform F2 the genesis of both types of heterotactic subfabrics is a linked process, where the direct componental movements reflect changes of the deformation conditions.

The differences in biotite subfabrics of both folds are evident also in domains of the fold knee, where the original fabric s_1 is best preserved. On both limbs of the antiform F2 in addition to biotite 1 parallel with the plane s_1, also biotite normal to this plane was found (1 % isoline at Y and 2 % isoline at Z on Fig. 15 and 17). In spite of the position it cannot be regarded for a typical posttectonic cross-mica as biotite 2.

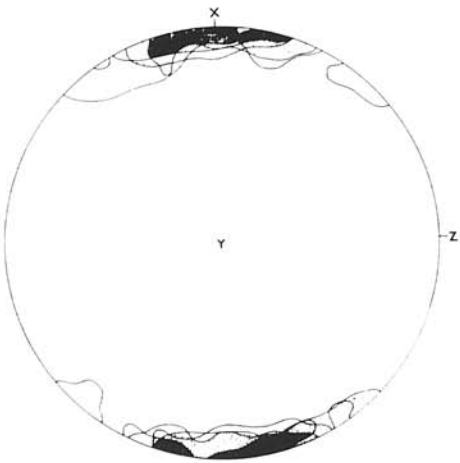

Fig. 21. Biotite, F2—1, 2, 3, 5, 6, synoptic diagram of 5 % isolines, 916 poles of {001}.

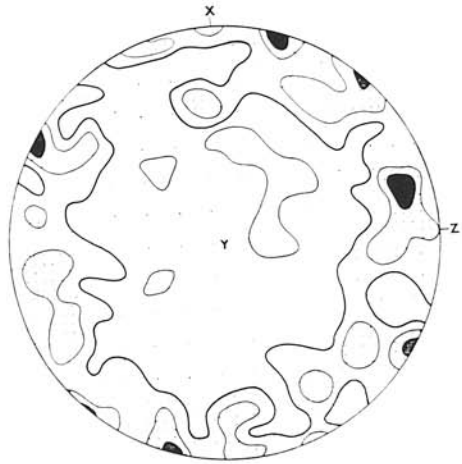

Fig. 22. Quartz, F1—1, 200 (0001), 0—1—2—3 < %.

Fig. 23. Quartz, F1—2, 200 (0001), 0—1—2—3 < %.

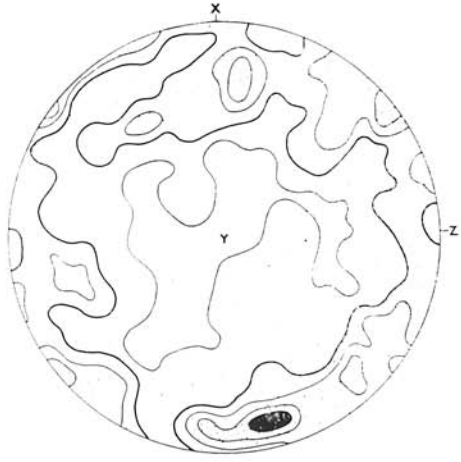

Fig. 24. Quartz, F1—3, 200 (0001), 0—1—2—3—4 < %.

In the synform F2 posterystalline deformation of biotite 1 has not been observed. The flakes are situated in s_1 — the 2 % isoline forms a pattern similar to B-tectonite, and sporadically in s_2 — the maxima in direction X (Fig. 18).

Subfabrics of quartz

The orientation of the optic axes of quartz 1 was measured on the same thin sections of both folds as the orientation of biotite. The orientation of the strain elipsoid axes was marked from the relevant diagram of biotite subfabric. The measured quartz 1 shows in both folds diverse time relations of crystallization to deformation.

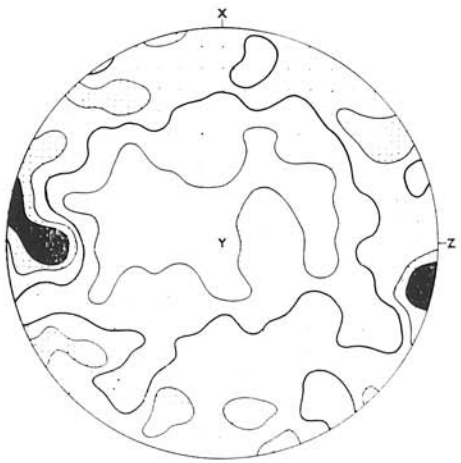

Fig. 25. Quartz, F1—4, 200 (0001), 0—1—2—3 < %.

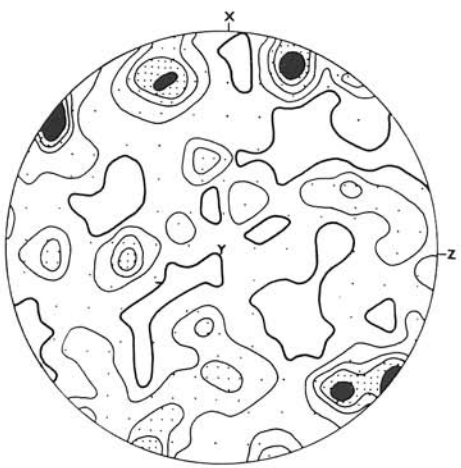

Fig. 26. Quartz, F2—1, 200 (0001), 0—1—2—3—4 < %.

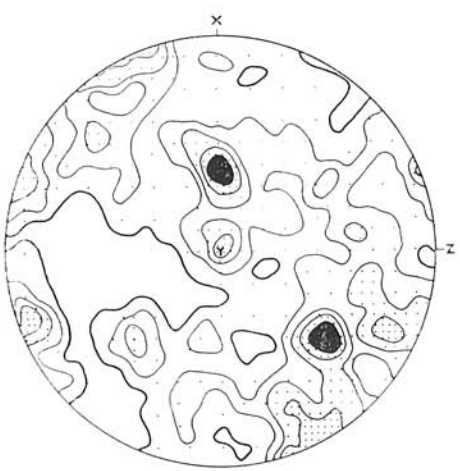

Fig. 27. Quartz, F2—2, 165 (0001), 0—1—2—3—4 < %.

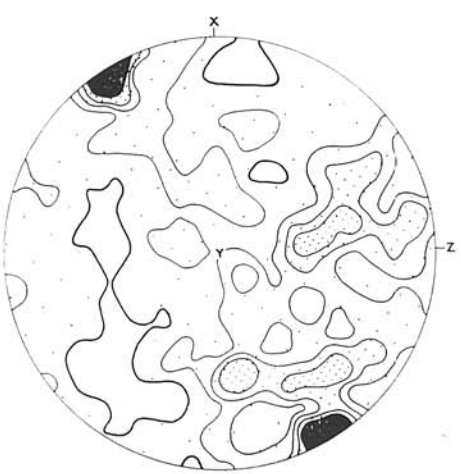

Fig. 28. Quartz, F2—3, 200 (0001), 0—1—2—3—4 < %.

In F1 quartz underwent deformation crystallizing originally during the formation of s_1 subfabric, or even during early stages of buckling. Its final fabric is the product of D_2. However the subordinate participation of relic fabrics cannot be eliminated.

In F2 quartz has been measured, which was crystallizing mainly synkinematically with the folding. Its fabric is primarily varying in the individual fold domains. The folding did in places and only unsubstantially overgrow the crystallization of quartz 1 (unlike F1). In domains devoid of posterystalline deformation the grain shape proves for crystallization by growth on sides of minimal stress, as it has been experimentally established by H. W. Fairbairn (1950).

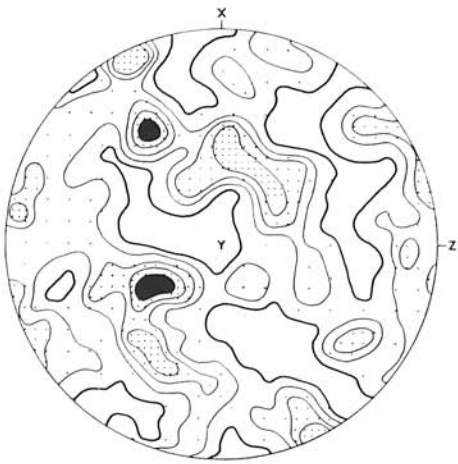

Fig. 29. Quartz, F2—4, 100 (0001), 0—1—2—3—4 < %.

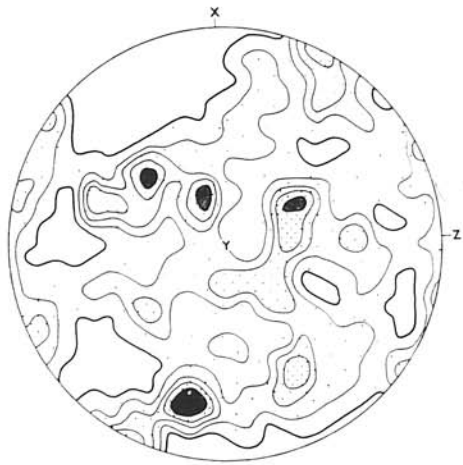

Fig. 30. Quartz, F2—5, 99 (0001), 0—1—2—3—4 < %.

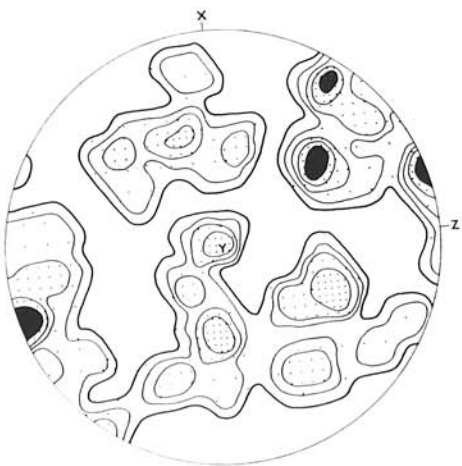

Fig. 31. Quartz, F2—6, 52 (0001), 0—1—2—4—6 < %.

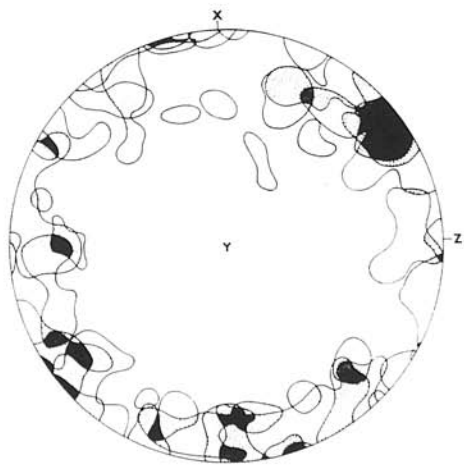

Fig. 32. Quartz, F1-1 to 4, synoptic diagram of 2 % isolines, 800 (0001).

Fold F1

The quartz diagrams (Fig. 22 to 25) have a common feature: the maximal density of the optic axes is near to the XZ-plane. The large circle of the 1 % isoline with the axis in Y occurs in three of the four diagrams. It is interrupted only in the fold hinge (Fig. 23). The position of the highest maximum to the Z-axis depends on the degree of preferred orientation of quartz by postcrystalline deformation. It is proportional to the actual or apparent homotaxis of both quartz and biotite subfabrics. The diagrams from the hinge and the lower limb correspond best to this rule (Fig. 23 and 25). The more intensive and homogenous is the effect of D_2 on quartz 1, the less are the maxima, which are cummulative and situated nearer to the Z-axis.

Fold F2

The apparently irregular distribution of the optic axes maxima reveals after more detailed study the following rule: towards the fold hinge the maximal concentrations migrate from the vicinity of the XZ-plane towards the Y-axis. In diagrams of the antiform limb and from the central limb the maxima lie on XZ (Fig. 26 and 28). In the lower limb near the core of the synform the highest maximum is in a distance of 42° from XZ (Fig. 31), in the antiform and synform cores it is up to 70° (Fig. 27, 29 and 30). The plot on Fig. 34 represents the position of the highest and other maxima with regard to XZ and Z.

The fabric of the quartz optic axes is in agreement with the diverse state of strain in the hinge and in the fold limbs. The buckling is accompanied by an expansion in the core into the direction of the fold axis (Y), in which the optic axes of quartz are gradually reoriented. The synform core is closest to this state, because in the antiform hinge zone creep set in in direction of the axial surface. On the fold limbs the orientation of quartz is controlled mainly by tangential longitudinal strain. On the diagrams from the central and synformal limb the maximum (or their group) lies in the direction of the convergent cleavage fan; the angle M∧X varies from 30° to 50°.

The migration of maxima of the quartz optic axes in F2, first of all in the synform hinge zone, reminds the stages leading to the ultimate steady-state pattern as they were determined by I. Hara (1971).

The subfabrics of quartz were tentatively unfolded in both folds according to the method of B. Sander (1930, 1950) and J. Ladurner (1950). The reduced homogeneity of the majority of subfabrics displaying by several maxima and their deviation from the ac-plane is a handicap. It has been partially overcome by the adoption of the highest maximum in the construction of the q-direction. Under these conditions F1 and F2 are in the sense of Sander's classification unhomo-

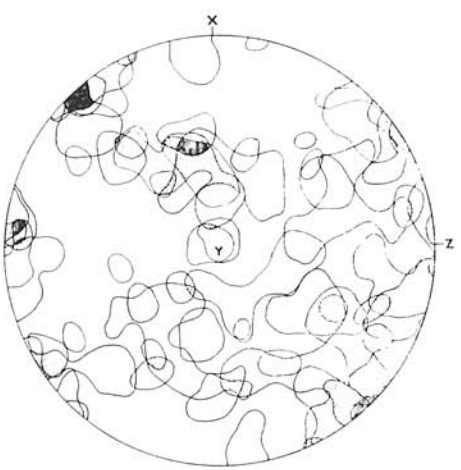

Fig. 33. Quartz, F2-1 to 6, synoptic diagram of 2 % isolines, 815 (0001).

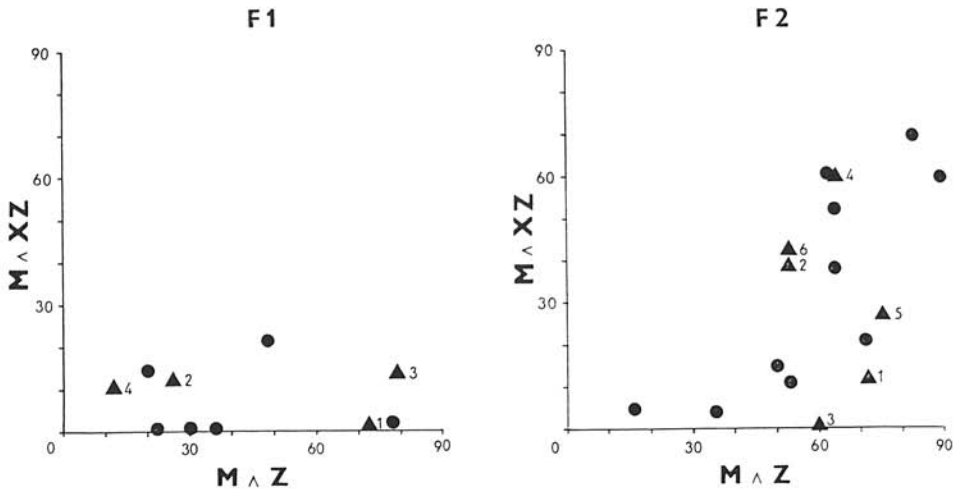

Fig. 34. Relationship between the angle M∧Z and M∧XZ for the highest (triangles) and the other maxima (points) on the quartz optic axes diagrams in F1 and F2.

geneously oriented folds without possibility of unfolding. Quartz fabric in F2 and migration of the maxima towards Y, recall a quartz phyllite fold from Brixen analyzed by I. Shafflerzozzmann (1955).

Comparison of fold fabrics and their structural regimes

By geometric and microscopic analyses, differences between both folds were found in the majority of the investigated phenomena. Differences in geometric features of folds are coherent to the state of strain, which depends on the rheologic properties of the deformed rocks. In F2 metamorphic differentiation conspicuously separated the biotite from those of quartz-feldspar layers, unlike of F1 where the dark layers are commonly of composite constitution. In the core and in the hinge zone of F2 antiform the effacement of metamorphic differentiation set in subsequently, due to intensive creep.

Compression of the fold arc F1 is smaller than in F2, as the decollement and creep in the antiform, resp. the impress of synform core indicate. The cross section shape of the F1 quartz-feldspar layers is more regular than that of F2, variations $t'\alpha$ of particular layer of F2 are larger than in F1. The biotite layers of F2 reduced by differentiation cannot be described by orthogonal thicknes. Their deformation is passive, closely related to the deformation of the quartz-feldspar layers. The layers of both folds, or their minor parts are frequently folded in the subclass 1C with weakly convergent isogons.

The differences in mineral composition of the rocks before folding are unsubstantial. More important are the differences in grain size influencing the course of recrystallization and creep. Grain size of the quartz-feldspar layers in F2 is 10 to 50 times larger than that of F1. The differences in mineral composition generate gradually with folding in the state of retrograde metamorphims. The crystallization of the retrograde mineral assemblages is induced in every fold by another mode. In F1 these are direct componental movements, penetrating most intensely the biotite layer of the outer arc, where they pass into indirect componental movements of retrograde crystallization. In F2 the

retrograde mineral assemblage occurs firstly in the domain of maximal compression and minimal direct componental movements (synform core). The direct componental movements in the antiform are not accompanied by retrograde crystallization.

The retrograde mineral assemblage of F1 is lower temperated as in F2. In both folds retrograde crystallization is allied to domains of a particular suitable original mineral composition and a particular fold section. This phenomenon is common in mesoscopic and macroscopic domains of the Tatroveporide crystalline complex.

The differences in biotite subfabrics of both folds are evident in the hinge zone. In F1 biotite 1 subfabric has been formed by direct componental movements, in F2 by indirect componental movements. In RMD of F2 in addition cross biotite 2 crystallized. In both folds the older planar fabric s_1 has been deformed by a mode adequate to the structural regime. Biotite subfabrics indicate not only the diverse formation of both folds, but also the different formation of the antiform and synform of F2. The fabric of the F2 synform originated likely in a deeper level and earlier as the fabric of the hinge zone of the antiform. The succesion of deformation in F2 is proved in this sense by the mesoscopically observed flexure of the axial surface.

Differences in quartz subfabrics of both folds are again most conspicuous in the hinge zones. They are characterized by the position of the optic axes towards the axes of the strain elipsoid. While in F1 the highest density of the optic axes is in the XZ-plane and near the Z-axis, in F2 it is far of XZ, implicating a small circle with the axis Y.

The mentioned differences in fabric of the investigated folds are due to the deformation during diverse structural regimes. The structural regime is a result of several factors, from which temperature, strain, time, chemical constitution of rocks and the presence of the fluid phase are most important and of mutual interaction. Quantitative and qualitative variations in the system of the structural regime induce intensive changes of the structural style. Comparing the deformation mechanism even of an individual mineral in both folds the complexity of the process is evident. Thus according to the criteria of D. Flinn (1965), the fold-forming deformation of biotite 1 in PMD of F1 was activated nonthermally, while in F2 it was activated thermally and nonthermally. The deformation of quartz 1 in the same domains of F1 was activated mostly nonthermally, of F2 thermally. The deformation of RMD is in both folds activated thermally (recrystallization). The mechanism of deformation is changing already in the grain domain and varies commonly in diverse layers and is always different in various fold domains. The determination of the structural regime can be approached by correlation of mesoscopic and microscopic structures with the metamorphic facies, as it was effectuated by J. G. Holland and R. St. Lambert (1969). According to the criteria they determined, F1 originated in regime 2 and F2 in regime 3. The classification is only approximate, owing to variations of mineral composition and strain variation within time and structure. They induce variations even in the range of the total regime within the domain of one fold. Its result is the convergency of structural regimes and corresponding fold style, as it is observable in one part of the investigated crystalline complex.

Conclusion

The mode of formation of two mesoscopic folds in metamorphites of Low Tatra Mts. Dumbier crystalline complex was approached by the study of morphology, mineral constitution and its fabric.

The differences in morphology of the cross section between both folds are rather due to degree of recrystallization and metamorphic differentiation during the deformation, than to the original mineral composition. Differences in geometric features of the individual layers of a certain fold are due to the diverse competency as a function of mineral composition. The variability of geometric properties of the fold from shallower level (F1) is lower than in the fold from the deeper level (F2). The modification of the fold shape is proportional to incompetency.

The fold F1 originated by deformation conspicuously separated temporarily from the prograde metamorphism of gneiss, while F2 was deformed simultaneously and closely after prograde metamorphism. In both folds the effects of retrograde metamorphism are consequent with the folding process, they revealed only in a certain structure domain with suitable mineral composition and state of strain.

Both folds generated by deformation of planar fabrics. Subfabrics of biotite and quartz characterize the various time sections of folding, the degree of their genecity varies with the position in the structure. The state of strain and the variations of the structural regime during folding demostrate the biotite and quartz subfabrics from the hinge domains. These in a fold from a shallower level are formed firstly by direct componental movements, unlike in the fold from the deeper structural level.

The studied aspects of fold fabrics point to the diversity of structural regimes under which they originated. It is evident that they represent only a part of the scale of deformation conditions created in the time-spatial plan of the Variscan and Alpine orogeny.

REFERENCES

DONATH, F. A. 1962: Role of layering in geologic deformation. Trans. N. Y. Acad. Sci. (New York), 2, 24, p. 236—249.

FAIRBAIRN, H. W. 1950: Synthetic quartzite. Amer. Mineralogist (Washington), 35, p. 735—748.

FLINN, D. 1965: Deformation in metamorphism. In: Controls of metamorphism. Geol. J. Spec. Issue (Edinburg—London), No. 1, p. 46—72.

HARA, I. 1971: An ultimate steady-state pattern of c-axis fabric of quartz in metamorphic tectonites. Geol. Rdsch. (Stuttgart), 60, No. 3, p. 1142—1173.

HOLLAND, J. G.—LAMBERT, R. ST. 1969: Structural regimes and metamorphic facies. Tectonophysics (Amsterdam), 7, No. 3, p. 197—217.

KANTOR, J. 1959: Príspevok ku geochronológii nizkotatranských granitoidov. Geol. práce (Bratislava), 55, p. 159—169.

KANTOR, J. 1961: Beitrag zur Geochronologie der Magmatite und Metamorphite des Westkarpatischen Kristallins. Geol. Práce (Bratislava), 60, p. 303—318.

LADURNER, J. 1950: Beiträge zur Typisierung von Quarzfalten. TMPM (Wien), 2, No. 1, p. 47—66.

RAMSAY, J. G. 1962: The geometry and mechanics of formation of „similar" type folds. J. Geol. (Chicago), 70, p. 309—327.

RAMSAY, J. G. 1967: Folding and fracturing of rocks. 1st ed., New York, McGraw-Hill Book Co., 568 p.

SANDER, B. 1930: Gefügekunde der Gesteine. Wien, Springer-Verlag, 352 p.

SANDER, B. 1950: Einführung in die Gefügekunde der geologischen Körper. Teil 2. Wien und Insbruck, Springer-Verlag, 409 p.

SCHAEFLER-ZOZMANN, I. 1955: Gefügeanalyse an Quarzfalten. N. Jb. Mineral. Abh. (Stuttgart), 87, No. 3, p. 321—350.

SIEGL, K. 1970: Štruktúrna analýza dumbierskeho kryštalinika. Manuscript, Geofond, Bratislava, 147 p.

Review by J. ŠTELCL.